

The Intricate Love Affairs between MoS 2 and Metallic Substrates

Velický, M., Donnelly, G. E., Hendren, W. R., DeBenedetti, W. J. I., Hines, M. A., Novoselov, K. S., Abruña, H. D., Huang, F., & Frank, O. (2020). The Intricate Love Affairs between MoS 2 and Metallic Substrates. *Advanced Materials Interfaces*. <https://doi.org/10.1002/admi.202001324>

Published in:
Advanced Materials Interfaces

Document Version:
Publisher's PDF, also known as Version of record

Queen's University Belfast - Research Portal:
[Link to publication record in Queen's University Belfast Research Portal](#)

Publisher rights

Copyright 2020 the authors.

This is an open access article published under a Creative Commons Attribution License (<https://creativecommons.org/licenses/by/4.0/>), which permits unrestricted use, distribution and reproduction in any medium, provided the author and source are cited.

General rights

Copyright for the publications made accessible via the Queen's University Belfast Research Portal is retained by the author(s) and / or other copyright owners and it is a condition of accessing these publications that users recognise and abide by the legal requirements associated with these rights.

Take down policy

The Research Portal is Queen's institutional repository that provides access to Queen's research output. Every effort has been made to ensure that content in the Research Portal does not infringe any person's rights, or applicable UK laws. If you discover content in the Research Portal that you believe breaches copyright or violates any law, please contact openaccess@qub.ac.uk.

The Intricate Love Affairs between MoS₂ and Metallic Substrates

Matěj Velický,* Gavin E. Donnelly, William R. Hendren, William J. I. DeBenedetti, Melissa A. Hines, Kostya S. Novoselov, Héctor D. Abruña, Fumin Huang,* and Otakar Frank*

Mechanical exfoliation yields high-quality 2D materials but is challenging to scale up due to the small lateral size and low yield of the exfoliated crystals. Gold-mediated exfoliation of macroscale monolayer MoS₂ and related crystals addresses this problem. However, it remains unclear whether this method can be extended to other metals. Herein, mechanical exfoliation of MoS₂ on a range of metallic substrates is studied. It is found that Au outperforms all the other metals in their ability to exfoliate macroscale monolayer MoS₂. This is rationalized by gold's ability to resist oxidation, which is compromised on other metals and leads to a weakened binding with MoS₂. An anomalously high monolayer yield found for Ag suggests that the large interfacial strain in the metal–MoS₂ heterostructures measured by Raman spectroscopy also is a critical factor facilitating the exfoliation, while the relative differences in the metal–MoS₂ binding play only a minor role. These results provide a new incentive for investigations of 2D material-substrate combinations applicable where high-quality 2D crystals of macroscopic dimensions are of importance.


Mechanical exfoliation of 2D materials yields high-quality crystals popular with researchers in fundamental scientific disciplines but its scalability is severely limited. This method

Dr. M. Velický, Dr. G. E. Donnelly, Dr. W. R. Hendren, Dr. F. Huang
 School of Mathematics and Physics
 Queen's University Belfast
 University Road
 Belfast BT7 1NN, UK
 E-mail: f.huang@qub.ac.uk

Dr. M. Velický, Prof. K. S. Novoselov
 Department of Physics and Astronomy
 University of Manchester
 Oxford Road, Manchester M13 9PL, UK
 E-mail: matej.velicky@manchester.ac.uk

Dr. M. Velický, Dr. W. J. I. DeBenedetti, Prof. M. A. Hines, Prof. H. D. Abruña
 Department of Chemistry and Chemical Biology
 Cornell University
 Ithaca, NY 14853, USA

Dr. O. Frank
 J. Heyrovský Institute of Physical Chemistry
 Czech Academy of Sciences
 Dolejšková 2155/3, Prague 182 23, Czech Republic
 E-mail: otakar.frank@jh-inst.cas.cz

 The ORCID identification number(s) for the author(s) of this article can be found under <https://doi.org/10.1002/admi.202001324>.

DOI: 10.1002/admi.202001324

generates 2D monolayers tens or hundreds of microns in lateral sizes on most substrates, often after an elaborate surface treatment.^[1] Gold-mediated exfoliation of chalcogenides, chlorides, thiophosphates, black phosphorus, and black arsenic, with a robust control of the near-unity monolayer yield at a millimeter-/centimeter-scale, has recently emerged as a viable solution to the scalability issues,^[2] and has been adopted in various branches of applied research and engineering.^[3] In the case of transition metal dichalcogenides (TMDCs), the root of the preferential monolayer exfoliation has been attributed to the strong interactions between gold and chalcogenides, which have been explored in different facets of science for decades.^[4] However, it has recently been shown that the interaction between TMDCs and Au is non-covalent and van der Waals

(vdW) in its nature, inferred from the sizeable S–Au equilibrium distance (3.5 Å) and binding energies in the Au–MoS₂ heterostructure.^[2c,5] The vdW interaction therefore facilitates the transfer of the TMDC monolayers onto non-metallic substrates, which restore their semiconducting characteristics exploitable in optoelectronics, photovoltaics, and related themes.^[2b] The polymer-free nature of this transfer, which leaves surfaces free from residual contamination, is of significant advantage also.^[6] Despite these research efforts, it is currently unknown whether this method can also be applied to other metals, predicted to exhibit even stronger binding with MoS₂ than Au.^[7]

Here, we study the ability of different metallic substrates to exfoliate large-area monolayer MoS₂. We find that gold is by far the best substrate, outperforming all other metals by at least two orders of magnitude in terms of the lateral size of the MoS₂, thanks to the unique ability of Au to resist oxidation and the sizeable interfacial strain in the Au–MoS₂ heterostructure. A moderate exfoliation yield is achieved for other precious metals, including Pt, Pd, and Ag, while hardly any exfoliated material is found on base metals, including Cu, Ni, Co, Cr, and Ti, which suffer from significant oxidation of their surface upon exposure to air. A correlation between the maximum lateral sizes of the exfoliated monolayers, nobility of the metallic substrates expressed by their standard redox potential, and extent of their surface oxidation quantified by X-ray photoelectron

spectroscopy (XPS) is found. Ag is an exception to this trend as it produces the largest monolayers among the non-Au precious metals, thanks to the large Ag–MoS₂ lattice mismatch, which introduces strain and facilitates monolayer exfoliation. Our results assert that both the metal nobility and interfacial strain are key for the large exfoliation yield and that the relative differences in the metal–MoS₂ binding energies are insignificant.

When a high-quality crystal source is used, the bulk TMDC acts as a stamp, preferentially exfoliating as a monolayer everywhere a good contact with the Au is achieved.^[2a-d,3] The critical factor for successful exfoliation is the cleanliness of the freshly deposited Au and freshly exfoliated TMDC, as exposure to air or prolonged periods spent under the ultra-high vacuum of the deposition chamber lead to accumulation of adventitious contamination and suppression of the high yield. We showed previously that the Au–MoS₂ binding energy, which facilitates monolayer exfoliation, decreases to a critically low level, comparable to the MoS₂–MoS₂ binding energy, when the Au surface is exposed to air for a few minutes.^[2c] Such a weakened interaction is expected for a mere 1 Å increase in the S–Au separation induced by the airborne organic contamination, known to plague most metallic and 2D surfaces.^[8]

Most other metals are predicted to bind with MoS₂ even more strongly than Au due to the shorter equilibrium distances

in their metal–MoS₂ heterostructures.^[7] One would therefore expect that they would produce high monolayer yields also. Nonetheless, the maximum lateral sizes of monolayer MoS₂ obtained on different metallic substrates shown in **Figure 1a** indicate that this is not the case. We categorized the metals into three groups based on the size of the monolayer MoS₂ they typically yield: negligibly small ($\approx 1 \mu\text{m}$ or less) on Cu, Ni, Co, Cr, and Ti; moderately-sized ($\approx 10\text{--}100 \mu\text{m}$) on Pt, Pd, and Ag; and extremely large ($\approx 1 \text{cm}$) on Au, at least two orders of magnitude larger than on any other substrate. The metals in **Figure 1a** are ordered according to their standard redox potential (right axis), which is the measure of their nobility and therefore ability to withstand oxidation. We conclude that the correlation between the lateral size of monolayer MoS₂ and the nobility of the metallic substrate is not accidental but is rooted in the formation of a metal oxide layer, which decreases the effective metal–MoS₂ binding and therefore reduces the exfoliation yield.

Crucially, the other (non-Au) precious metals with standard redox potentials above +0.8 V (Pt, Pd, and Ag) all yield MoS₂ monolayers comparable in size to those exfoliated on non-metallic substrates such as SiO₂ or polymethyl methacrylate,^[11] large enough to meet the needs of fundamental research (**Figure 1b**). The XPS survey of the bare Au, Pt, and Ag substrates in **Figure 1c** allowed us to determine the amount of

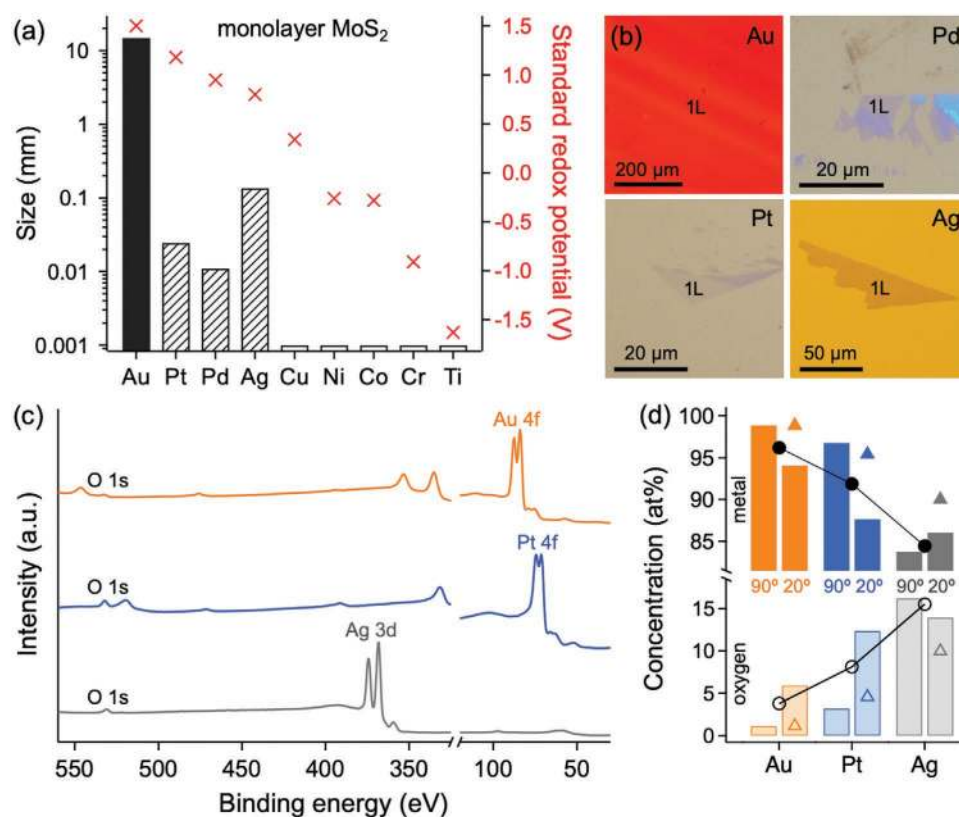


Figure 1. Metallic substrates for mechanical exfoliation of MoS₂. a) The maximum lateral sizes of mechanically exfoliated monolayer MoS₂ ordered according to the standard redox potential (vs standard hydrogen electrode) of the metallic substrate.^[9] b) Optical images of monolayer MoS₂ (1L) on 7 nm Au, Pt, Pd, and Ag, deposited on a 90 nm SiO₂/Si support using a 3 nm Ti adhesion layer. c) XPS survey of bare Au, Pt, and Ag obtained at 20° take-off angle between the photoelectrons and sample surface. d) Metal (full color) and oxygen (desaturated color) concentrations quantified from the Au 4f, Pt 4f, Ag 3d, and O 1s core levels of the XPS surveys obtained at 90° and 20° take-off angles, using sensitivity factors from ref. [10]. Black circles denote concentrations averaged over both take-off angles and colored triangles are concentrations corrected for the O 1s multi-peak fitting (20° only).

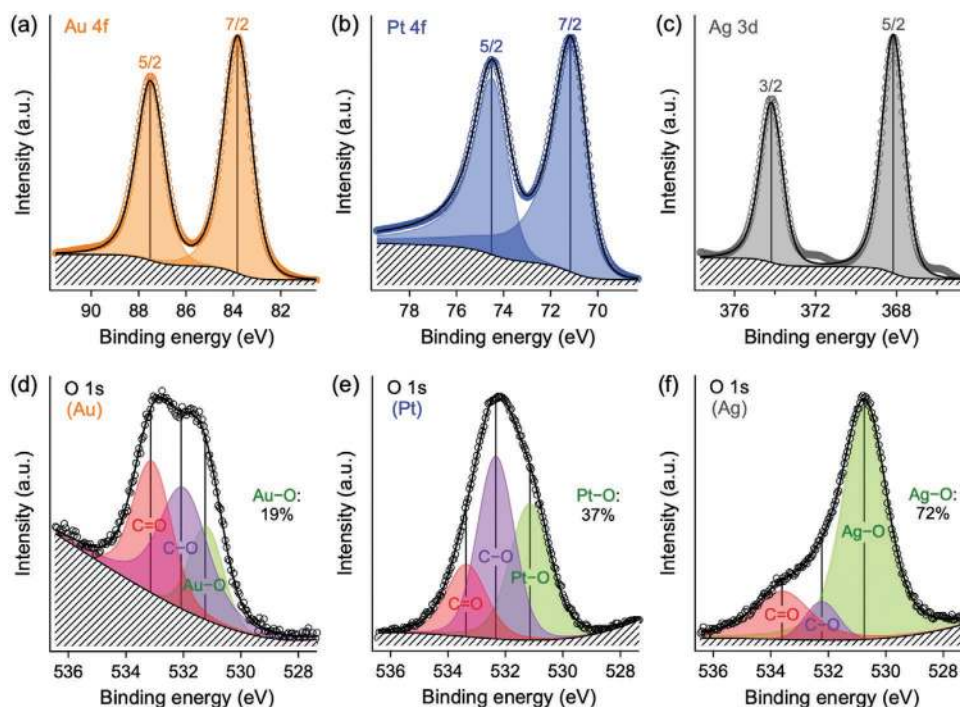


Figure 2. High-resolution XPS of the metallic substrates. a–c) Au 4f, Pt 4f, and Ag 3d core-level spectra acquired on bare Au, Pt, and Ag at glancing emission (20° take-off angle). The satellite peak at c) 366 eV arises from a minor X-ray line of the non-monochromated source and the energy loss peaks at 372 and 378 eV correspond to the Ag plasmon.^[12a] d–f) Corresponding O 1s core levels on these substrates at glancing emission.

surface metal and oxygen from the Au 4f, Pt 4f, Ag 3d, and O 1s core levels. The metal concentrations in Figure 1d, determined from the XPS surveys are proportional to their standard redox potential. A comparison of the data obtained at normal and glancing emission (90° and 20° take-off angle) shows that the oxygen concentration in Au and Pt is significantly enhanced in the near-surface region, which is consistent with oxidation being a surface process. The oxygen concentrations in Ag are similar for both emission conditions, most likely due to the deeper extent of the oxide layer.

High-resolution XPS analysis allowed us to distinguish between metal oxidation and oxygen-containing organic contaminants. Due to the low oxygen concentration, none of the metal core level spectra (Au 4f, Pt 4f, Ag 3d) shown in Figure 2a–c exhibit oxidation-related features, common for the base metals in this study.^[12] In contrast, the O 1s spectra on all three metals showed characteristic broadening due to the presence of both metal oxides and adventitious carbonaceous contaminants, such as alcohols and acids. The O 1s glancing emission spectra in Figure 2d–f were fitted to three components, corresponding to organic oxygen (both C=O at 533.1–533.5 eV and C–O at 532.0–532.3 eV) and oxidized metal (M–O at 530.7–531.2), where M = Au, Pt, or Ag.^[8d,13] The percentage of oxygen chemisorbed as M–O increases from 19% on Au, to 37% on Pt, and 72% on Ag. This analysis showed that 1% of the Au surface, 5% of the Pt surface, and 10% of the Ag surface was oxidized (colored triangles in Figure 1d), representing the oxygen concentrations originating only from M–O.

The XPS confirms that the resistance to oxidation gives gold a significant advantage over all other metals, whose effective metal–MoS₂ binding is weakened and monolayer MoS₂ yield

reduced by the formation of the metal oxide layer. However, Figure 1a indicates that Ag facilitates exfoliation of sizeable MoS₂ monolayers, about one order of magnitude larger than on Pt and Pd, deviating from the size-nobility trend. Considering the higher propensity of Ag for oxidation than Pt and Pd, another factor must be responsible for such an anomaly. Figure 3a shows the Raman spectra of monolayer MoS₂ on Au, Ag, Pt, Pd, relative to that on SiO₂. The downshifts of the out-of-plane E' Raman modes on all metallic substrates indicate tensile strain in MoS₂,^[14] and their overall width and asymmetry reflect the varying levels of strain distribution. For purposes of the substrate comparison, we disregard the possible effects of charge doping, which causes E' mode shifts smaller than 1 cm^{-1} for the charge carrier density up to nearly 10^{14} cm^{-2} .^[15] The strain median, which was chosen to capture the mean values of the diverse E' mode shapes in Figure 3a, increases from 0.7% on Pd, to 1.3% on Pt, 1.4% on Ag, and 1.5% on Au. The E' mode on Au is nearly symmetric and fittable with a single Voigt line shape but broader than on SiO₂ (cf. linewidths of 6.1 vs 2.4 cm^{-1}). The resulting strain dispersion, expressed as the interquartile range (IQR) between the first (Q_1) and third (Q_3) quartile of the distribution (*i.e.*, 25th and 75th percentile, respectively), is 1.0%. In contrast, the E' modes on Ag and Pt are notably asymmetric and broader than those on Au with IQRs of 1.7% and 1.3%, respectively, and require fitting with at least two Voigt components with largely varied linewidths. Crucially, the maximum strain levels reached on Ag ($Q_3 = 2.4\%$) are larger than on Pt ($Q_3 = 2.0\%$), and on Pd ($Q_3 = 1.3\%$).

The measured strain values are in agreement with previous experimental observations^[16] and consistent with the relative strains applied theoretically to metals in order to relax the

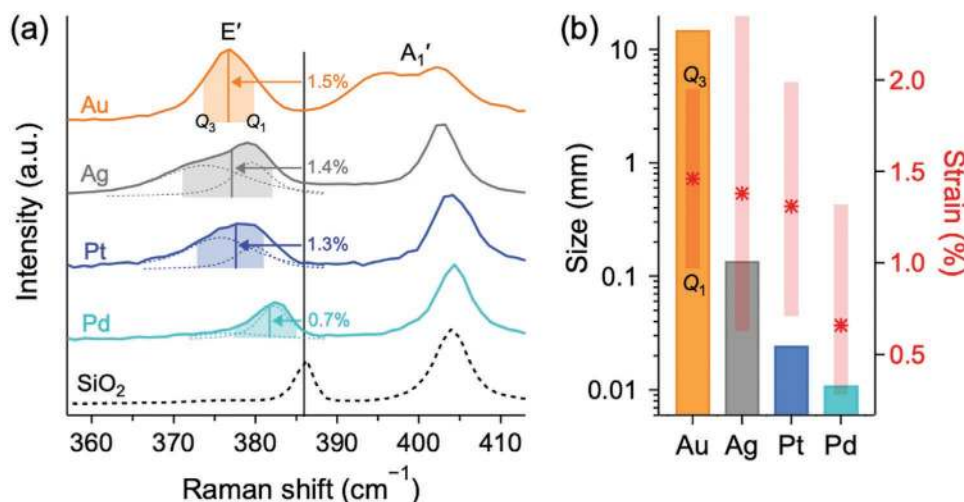


Figure 3. Strain analysis of the metal–MoS₂ interface. a) Raman spectra of monolayer MoS₂ on Au, Ag, Pt, and Pd, compared to that on SiO₂. The vertical lines and shaded ranges encompassing them represent strain medians (Q_2) and lower/upper quartiles (Q_1/Q_3), respectively, derived from the E' modes relative to SiO₂^[14] by integrating the area under the fitted curve (using a single peak for Au and sum of two peaks for the other metals). b) Correlation between the lateral size and the metal-induced tensile strain of monolayer MoS₂.

lattice mismatch in their metal–MoS₂ heterostructures.^[7a] This has recently been rationalized theoretically, showing that both tensile and compressive biaxial strains induced by the substrate promote monolayer exfoliation due to the energetically unfavorable disruption of the interlayer AB stacking registry in bulk MoS₂.^[17] Our data suggest that the oxide-free Au surface facilitates uniform strain and therefore binding with MoS₂ wherever the two materials are in contact. Conversely, the larger strain dispersion on Ag and Pt reflects their higher susceptibility to oxidation and potentially spatial heterogeneity of the strain. In the particular case of Ag, the two-component fitting of the E' mode yields a low-frequency peak corresponding to 1.8% of strain. Indeed, such a high maximum strain likely facilitates the local mechanical pinning of MoS₂ on Ag, leading to an exfoliation yield higher than expected from Ag's propensity for oxidation. Correlation between the lateral size of monolayer MoS₂ and the induced strain shown in Figure 3b therefore suggests that, along with the oxidation resistance, large uniform interfacial strain is one of the main drivers behind the preferential monolayer exfoliation. These two critical factors determine the effective strength of the metal–MoS₂ interaction and the resulting monolayer yield. Furthermore, it appears that the relative differences in the binding energies of different metal–MoS₂ heterostructures are secondary, since the Au–MoS₂ binding actually is one of the weakest among the metals studied here.^[7]

Our results affirm that gold is a substrate uniquely suited for preferential mechanical exfoliation of macroscopic monolayers MoS₂ and other TMDCs due to its exceptional ability to withstand oxidation. All other metals have a lower nobility than gold and suffer from partial oxidation of their surface, which weakens the metal–MoS₂ binding. The non-Au precious metals, including Pt, Pd, and Ag, produce moderately-sized monolayers, satisfactory for most research applications. Crucially, Ag exhibits anomalously high yield relative to its lower nobility, which indicates that the sizeable interfacial strain of the metal–MoS₂ heterostructure also is key for successful exfoliation. Other base metals, including Cu, Ni, Co, Cr, and Ti,

have a negligible monolayer yield due to the significant oxidation of their surface. These observations confirm that the oxidation resistance and large interfacial strain are the two dominant factors facilitating the preferential monolayer exfoliation, while the relative differences in theoretical metal–MoS₂ binding have a negligible effect. Our results provide a new stimulus towards the search for optimal combinations of 2D materials and suitable substrates, exploitable in macroscale electronic, photonic, or catalytic applications.

Experimental Section

All metals were deposited on a 90 nm SiO₂/Si support using a CMS-A DC magnetron sputterer (Kurt J Lesker Company Ltd) or an SC4500 e-beam evaporator (CVC Products Inc), both housing oil-free pumps. The metal thickness was monitored in situ using a quartz crystal or determined ex situ by X-ray reflectometry using a D8 Discover diffractometer (Bruker Inc). Bulk natural molybdenite (MoS₂), provided by Manchester Nanomaterials Ltd, was exfoliated using the Scotch-tape technique directly onto freshly deposited metallic substrates. The optical images were taken using a Nikon L200N Eclipse microscope. XPS was measured using an Omicron DAR 400 system with a non-monochromated Mg K α anode and calibrated using an Ag standard. The photoelectrons were collected at the surface normal (90° take-off angle) and glancing emission (20° take-off angle) using a Sphera II hemispherical analyzer. The metal substrates were exposed to air for no more than 6 h prior to the XPS characterization. Raman spectra were measured using an inVia Renishaw spectrometer equipped with a 532 nm laser excitation and 2400 l/mm grating.

Acknowledgements

This project has received funding from the European Union's Horizon 2020 research and innovation programme under the Marie Skłodowska-Curie grant agreement No. 746685, EPSRC (grant No. EP/N025938/1), and Seagate Technology (Ireland) under SOW #00077300.0. This work was performed in part at the Cornell NanoScale Science & Technology Facility, a member of the National Nanotechnology Coordinated

Infrastructure, which is supported by the NSF (Grant NNCI-1542081), and made use of the Cornell Center for Materials Research Shared Facilities, which are supported through the NSF MRSEC program (DMR-1719875). O.F. acknowledges the support of the Czech Science Foundation project No. GACR 17–18702S.

Conflict of Interest

The authors declare no conflict of interest.

Keywords

mechanical exfoliation, metallic substrates, MoS₂, strains, surface oxidation

Received: July 27, 2020

Revised: September 20, 2020

Published online:

- [1] Y. Huang, E. Sutter, N. N. Shi, J. Zheng, T. Yang, D. Englund, H.-J. Gao, P. Sutter, *ACS Nano* **2015**, *9*, 10612.
- [2] a) G. Z. Magda, J. Pető, G. Dobrik, C. Hwang, L. P. Biró, L. Tapasztó, *Sci. Rep.* **2015**, *5*, 14714; b) S. B. Desai, S. R. Madhupathy, M. Amani, D. Kiriya, M. Hettick, M. Tosun, Y. Zhou, M. Dubey, J. W. Ager, D. Chrzan, A. Javey, *Adv. Mater.* **2016**, *28*, 4053; c) M. Velický, G. E. Donnelly, W. R. Hendren, S. McFarland, D. Scullion, W. J. I. DeBenedetti, G. C. Correa, Y. Han, A. J. Wain, M. A. Hines, D. A. Muller, K. S. Novoselov, H. D. Abruña, R. M. Bowman, E. J. G. Santos, F. Huang, *ACS Nano* **2018**, *12*, 10463; d) Y. Huang, Y.-H. Pan, R. Yang, L.-H. Bao, L. Meng, H.-L. Luo, Y.-Q. Cai, G.-D. Liu, W.-J. Zhao, Z. Zhou, L.-M. Wu, Z.-L. Zhu, M. Huang, L.-W. Liu, L. Liu, P. Cheng, K.-H. Wu, S.-B. Tian, C.-Z. Gu, Y.-G. Shi, Y.-F. Guo, Z. G. Cheng, J.-P. Hu, L. Zhao, G.-H. Yang, E. Sutter, P. Sutter, Y.-L. Wang, W. Ji, X.-J. Zhou, H.-J. Gao, *Nat. Commun.* **2020**, *11*, 2453; e) L. Guan, B. Xing, X. Niu, D. Wang, Y. Yu, S. Zhang, X. Yan, Y. Wang, J. Sha, *Chem. Commun.* **2018**, *54*, 595.
- [3] a) H. M. Gramling, C. M. Towle, S. B. Desai, H. Sun, E. C. Lewis, V. D. Nguyen, J. W. Ager, D. Chrzan, E. M. Yeatman, A. Javey, H. Taylor, *ACS Appl. Electron. Mater.* **2019**, *1*, 407; b) V. Nguyen, H. Gramling, C. Towle, W. Li, D.-H. Lien, H. Kim, D. C. Chrzan, A. Javey, K. Xu, J. Ager, H. Taylor, *J. Micro Nano-Manuf.* **2019**, *7*, 041006; c) F. Liu, W. Wu, Y. Bai, S. H. Chae, Q. Li, J. Wang, J. Hone, X.-Y. Zhu, *Science* **2020**, *367*, 903.
- [4] a) D. J. Lavrich, S. M. Wetterer, S. L. Bernasek, G. Scoles, *J. Phys. Chem. B* **1998**, *102*, 3456; b) C. K. Yee, A. Ulman, J. D. Ruiz, A. Parikh, H. White, M. Rafailovich, *Langmuir* **2003**, *19*, 9450; c) H. Häkkinen, *Nat. Chem.* **2012**, *4*, 443.
- [5] S. G. Sørensen, H. G. Füchtbauer, A. K. Tuxen, A. S. Walton, J. V. Lauritsen, *ACS Nano* **2014**, *8*, 6788.
- [6] A. Krayev, C. S. Bailey, K. Jo, S. Wang, A. Singh, T. Darlington, G.-Y. Liu, S. Gradecak, P. J. Schuck, E. Pop, D. Jariwala, *ACS Appl. Mater. Interfaces* **2019**, *11*, 38218.
- [7] a) C. Gong, L. Colombo, R. M. Wallace, K. Cho, *Nano Lett.* **2014**, *14*, 1714; b) M. Farmanbar, G. Brocks, *Phys. Rev. B* **2016**, *93*, 085304; c) H. Zhong, R. Quhe, Y. Wang, Z. Ni, M. Ye, Z. Song, Y. Pan, J. Yang, L. Yang, M. Lei, J. Shi, J. Lu, *Sci. Rep.* **2016**, *6*, 21786.
- [8] a) T. Smith, *J. Colloid Interface Sci.* **1980**, *75*, 51; b) M. Velický, M. A. Bissett, P. S. Toth, H. V. Patten, S. D. Worrall, A. N. J. Rodgers, E. W. Hill, I. A. Kinloch, K. S. Novoselov, T. Georgiou, L. Britnell, R. A. W. Dryfe, *Phys. Chem. Chem. Phys.* **2015**, *17*, 17844; c) Z. Peng, R. Yang, M. A. Kim, L. Li, H. Liu, *RSC Adv.* **2017**, *7*, 27048; d) S. Sinha, M. Mukherjee, *Vacuum* **2018**, *148*, 48.
- [9] J. R. Rumble, *CRC Handbook of Chemistry and Physics*, C. R. C. Press, Boca Raton, FL **2019**.
- [10] C. D. Wagner, L. E. Davis, M. V. Zeller, J. A. Taylor, R. H. Raymond, L. H. Gale, *Surf. Interface Anal.* **1981**, *3*, 211.
- [11] a) A. Castellanos-Gomez, V. Singh, H. S. J. van der Zant, G. A. Steele, *Ann. Phys.* **2015**, *527*, 27; b) M. Velický, M. A. Bissett, C. R. Woods, P. S. Toth, T. Georgiou, I. A. Kinloch, K. S. Novoselov, R. A. W. Dryfe, *Nano Lett.* **2016**, *16*, 2023.
- [12] a) J. F. Moulder, W. F. Stickle, P. E. Sobol, K. D. Bomben, *Handbook of X-ray Photoelectron Spectroscopy*, Perkin-Elmer Corporation, Eden Prairie, Minnesota, USA **1992**; b) M. C. Biesinger, L. W. M. Lau, A. R. Gerson, R. S. C. Smart, *Appl. Surf. Sci.* **2010**, *257*, 887; c) M. C. Biesinger, B. P. Payne, A. P. Grosvenor, L. W. M. Lau, A. R. Gerson, R. S. C. Smart, *Appl. Surf. Sci.* **2011**, *257*, 2717.
- [13] G. Beamson, D. Briggs, *High Resolution XPS of Organic Polymers: The Scienta ESCA300 Database*, Wiley, New York **1992**.
- [14] a) A. Michail, N. Delikoukos, J. Parthenios, C. Galiotis, K. Papagelis, *Appl. Phys. Lett.* **2016**, *108*, 173102; b) D. Lloyd, X. Liu, J. W. Christopher, L. Cantley, A. Wadehra, B. L. Kim, B. B. Goldberg, A. K. Swan, J. S. Bunch, *Nano Lett.* **2016**, *16*, 5836.
- [15] a) Z. Melnikova-Kominkova, K. Jurkova, V. Vales, K. Drogowska-Horná, O. Frank, M. Kalbac, *Phys. Chem. Chem. Phys.* **2019**, *21*, 25700; b) B. Chakraborty, A. Bera, D. V. S. Muthu, S. Bhowmick, U. V. Waghmare, A. K. Sood, *Phys. Rev. B* **2012**, *85*, 161403; c) T. Sohler, E. Ponomarev, M. Gibertini, H. Berger, N. Marzari, N. Ubrig, A. F. Morpurgo, *Phys. Rev. X* **2019**, *9*, 031019.
- [16] a) C. Gong, C. Huang, J. Miller, L. Cheng, Y. Hao, D. Cobden, J. Kim, R. S. Ruoff, R. M. Wallace, K. Cho, X. Xu, Y. J. Chabal, *ACS Nano* **2013**, *7*, 11350; b) Y. A. Moe, Y. Sun, H. Ye, K. Liu, R. Wang, *ACS Appl. Mater. Interfaces* **2018**, *10*, 40246; c) M. Velický, A. Rodriguez, M. Bouša, A. V. Krayev, M. Vondráček, J. Honolka, M. Ahmadi, G. E. Donnelly, F. Huang, H. D. Abruña, K. S. Novoselov, O. Frank, *J. Phys. Chem. Lett.* **2020**, *11*, 6112; d) S. Yasuda, R. Takahashi, R. Osaka, R. Kumagai, Y. Miyata, S. Okada, Y. Hayamizu, K. Murakoshi, *Small* **2017**, *13*, 1700748.
- [17] H. Sun, E. W. Sirott, J. Mastandrea, H. M. Gramling, Y. Zhou, M. Poschmann, H. K. Taylor, J. W. Ager, D. C. Chrzan, *Phys. Rev. Mater.* **2018**, *2*, 094004.